中國機械工程學刊第四十六卷第一期第 63~72 頁(民國一百一十四年)
Journal of the Chinese Society of Mechanical Engineers, Vol.46, No.1, pp63~72 (2025)

Investigation on the Sliding Wear Characteristics of Ball Bearing Rolling Body under Starved Lubrication

Zhong-Tang Huo*, Jian-Qi Chen**, Ling-Juan Hao*** and Jian-Song Gao***

Keywords： starved lubrication, dynamic model, wear, bearing.

ABSTRACT

The long-term operation of ball bearing leads to the deterioration of lubrication condition, resulting in starved lubrication, which intensifies the wear of rolling body(RB). Accurately identifying this fault has a significant impact on bearing condition monitoring. In this paper, the wear of RB was quantified by diameter difference, and the friction between components was considered, the fault dynamic model of RB wear under the condition of starved lubrication was established. Simulation and experimental results indicated that an increase in starved lubrication could suppress the sliding effect, but the increased friction would exacerbate the wear of the RB; The fractional multiple of the rotation frequency of the cage in the frequency domain could be used as a basis for monitoring the degree and number of RB wear. In addition, changes in the degree of starved lubrication would directly affect the rotation frequency of the cage. However, the fractional multiple of the rotation frequency of the cage could still be used to identify RB wear fault. The proposal and validation of the model provide valuable references for achieving precise monitoring and qualitative diagnosis of bearings in actual working conditions.

INTRODUCTION

Rolling bearings are important supporting products in modern manufacturing and industrial production fields, are widely used in various fields of engineering machinery, its operation can effectively reduce the friction load, and its operational stability is of great significance to the entire mechanical system (Cao et al., 2019; Visnadi et al., 2019). Lubricants are the structure and working conditions that cannot be ignored during the use of bearings. In many special cases, due to untimely refueling or environmental factors, the lubricant deteriorates, which will cause the bearings to enter a state of starved lubrication. When the RB and the raceway are in the starved lubrication state, the asperity contact between the RB and the raceway will increase, which will easily lead to the increase of the bearing friction heat and serious wear (Wang et al., 2018; Wen et al., 2023). Hence, enhancing the precision of diagnosing bearings operating under lubrication deprivation is essential in situations where it is challenging to prevent such conditions in extreme work environments.

Creating mathematical models is an efficient way to elucidate the working principles of various states in bearings (Zhang et al, 2022; Wu et al, 2020). Qin (Qin et al., 2019) considering the coupling effect and segmentation effect of RBs, the influence of rotational speed and local defect size on vibration trend was quantified, and the rationality of the dynamic model method was verified. Jiang (Jiang et al., 2019) examined the abrupt shift in contact force that results in a sudden alteration in vibration, a phenomenon that is effectively investigated using dynamic modeling techniques. Changes in the interaction forces between bearing components can have an effect on the defect frequency. However, for the wear fault of RBs, it cannot be simply defined as a defect fault, but should be studied based on changes in size or spherical roundness. The above research clearly has low applicability

Lubrication is an important factor affecting the friction performance and operating status of bearings, Liu (Liu et al., 2020) established a dynamic model of rolling bearing and studied the effect of lubricant type on the dynamic characteristics of bearings. Shi (Shi et al., 2022) developed a numerical friction dynamics

Paper Received June, 2024. Revised September, 2024. Accepted October, 2024. Author for Correspondence: Jian-Qi Chen.

* *Associate Professor, Mechanical and Electrical College, Handan University, Handan, Hebei 056000, China,*

** *lecturer, Mechanical and Electrical College, Handan University, Handan, Hebei 056000, China, E-mail:chenjianqi1106@163.com.*

*** *lecturer, Mechanical and Electrical College, Handan University, Handan, Hebei 056000, China..*

analysis program to investigate the relationship between the state of lubrication and the tribological behavior of ball bearings. However, the discussion on starved lubrication is a new exploration based on the theory of elastohydrodynamic lubrication(EHL). Maruyama (Maruyama et al., 2015) studied the relationship between the oil supply flow rate and the oil film thickness under the condition of poor oil lubrication. Bian (Bian et al., 2021) considered the influence of insufficient lubrication conditions on the bearing performance, and showed that when the lubricant oil supply was insufficient, the bearing was in the starved lubrication state, and the bearing bearing capacity of the oil film was reduced, which easily led to bearing motion instability and wear. Shi (Shi et al., 2022) developed a friction dynamics analysis model, which can be used to evaluate the lubrication and wear status of bearings, becoming the theoretical basis for establishing a friction lubrication model in this paper. And for the research on RBs, Tu (Tu et al., 2021) examined the friction and contact forces between the RB and the raceway, and developed a dynamic model for the sliding of cylindrical roller bearings. Bai (Bai et al., 2019) pointed out that uneven loading caused by ceramic manufacturing errors is a typical fault of bearings, and established a dynamic model suitable for all ceramic ball bearings considering RB size errors. The results showed that RB size errors can cause increased friction and impact between all ceramic ball bearing components, and increased radiation noise. Shi (Shi et al., 2020) simulated the contact between the ball and the ring under non-uniform loading conditions. Simulation and experimental results show that the non-uniform loading situation varies with the diameter tolerance and arrangement of the RB, and the characteristic frequency of the RB raceway contact shifts from f_c to f_c', 2f_c', and 3f_c'. The above research indicates that the dynamic model considering the ball diameter difference of bearing RBs has good accuracy. By relying on the idea of ball diameter difference, it can be used to evaluate the phenomenon of uniform wear of RBs, and provide valuable materials for the study of dynamic models of RB wear in this paper.

From the above analysis, it can be seen that sufficient attention should be paid to bearings with wear fault of RBs under starved lubrication. To obtain the dynamic response of bearing with RB wear fault under starved lubrication condition, this paper calculated the changes in roughness contact ratio and contact force under different degrees of starved lubrication. The influence of structural parameters such as RB diameter tolerance and arrangement on load conditions was considered, and a dynamic model of bearing with RB wear fault under starved lubrication was established. Among them, Chapter 2 provided a detailed introduction to the established dynamic model. In Chapter 3, the characteristic frequencies of RB wear fault under starved lubrication were obtained, and the influence of starved lubrication level on fault characteristics was discussed. In Chapter 4, the calculated values were compared with the experimental results for verification. This study is helpful for the fault diagnosis and status monitoring of related equipment.

ESTABLISHMENT OF DYNAMIC MODEL FOR ROLLING BODY WEAR FAULT UNDER STARVED LUBRICATION

As shown in Fig.1, the coordinate system OYZ was set as the inertial coordinate system, $O_iY_iZ_i$ represented the center of mass coordinate system of the inner ring, and $O_jY_jZ_j$ represented the center of mass coordinate system of the jth RB. This article assumes that the outer ring of the bearing is in an interference fit with the bearing seat and fixed in place. Under raceway control, the RB rotates at an angular velocity of ω_{rj} and revolves around the outer ring axis at an angular velocity of ω_{mj}, while the cage rotates around the outer ring axis at an angular velocity of ω_c. ϕ_j is the azimuth angle of the jth RB in the coordinate system $O_iY_iZ_i$, and ψ_j is the azimuth angle of the jth RB in the coordinate system OYZ.

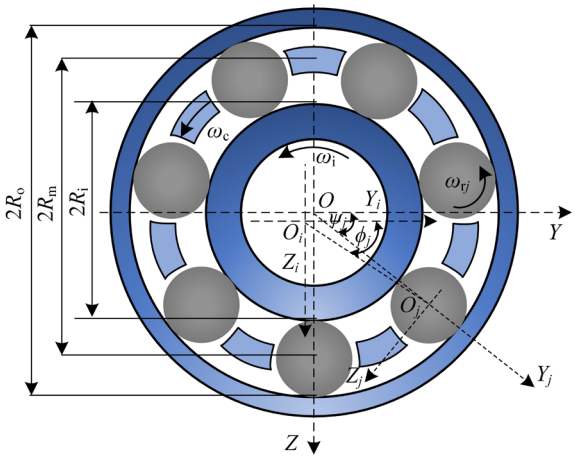

Fig. 1. Schematic of rolling bearing.

The azimuth ψ_j of the jth RB can be expressed as:

$$\psi_j = \omega_{mj} t + \theta_j + \frac{2\pi(j-1)}{N_b} \tag{1}$$

The diameter of the RB decreases after wear, and its load-bearing performance changes. D_j is the diameter of the RB, therefore, the relationship between ϕ_j and ψ_j is (Shi et al., 2020):

$$\psi_j = \phi_j + \arccos\frac{R_o^2 + R_i^2 - D_j(R_o - R_i) + D_j^2/2 - e^2}{2R_oR_i + D_j(R_o - R_i) - D_j^2/2} \tag{2}$$

Where e is the eccentricity.

The deformation and force relationship between the RB and the raceway are as follows (Liu et al., 2023):

$$\delta_j = \left| y\cos\phi_j + z\sin\phi_j - 0.5\lambda - \left(D_j - D_b\right)\right|_+ \quad (3)$$

Where "+" indicates that the equation takes only positive values; The contact force can be expressed as (Liu et al., 2023):

$$\begin{cases} Q_{ij} = K\beta\delta_j^{1.5} \\ Q_{oj} = K\beta\delta_j^{1.5} + m_r R_m \omega_{mj}^{\ 2} \end{cases} \quad (4)$$

Where: K is the equivalent contact stiffness (Wang et al., 2022); β is the switching function, take 1 when $\delta_j \geq 0$, otherwise it is 0.

Set the bearing area to cover the lower 1/3 symmetrical part of the bearing, as shown in Fig.2. Due to the uneven wear on each RB, there is a difference between the actual ball diameter value and the nominal diameter of the RB. Therefore, when the RB comes into contact with both the inner and outer rings, it is considered a load-bearing RB. Otherwise, the RB is considered to be moving along the outer ring raceway.

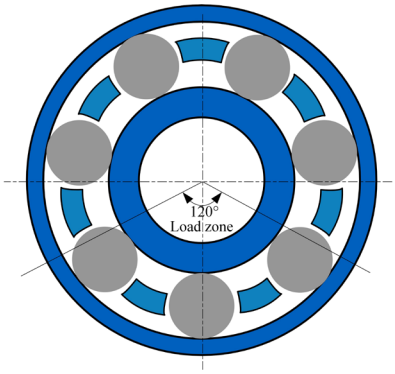

Fig. 2 Schematic of bearing bearing area

When the bearing area is uniformly loaded, the number of loaded RBs $N=N_b/3$, and the number of RBs in the bearing studied in this paper is $N_b=7$. Based on Fig.3, it can be seen that the number of loaded RBs in the bearing area varies between 2 and 3 without considering the difference in ball diameter. When there is wear on the RB, that is, when there is a difference in the ball diameter of the RB, the ball diameter of the RB satisfies:

$$D_j = D_n + A_j \cdot \delta \quad (5)$$

Where A_j is the diameter coefficient corresponding to the jth RB, and δ is the amplitude of the diameter difference.

When the jth RB passes through the bearing area and $D_{j\lim}$ is given, the critical value for determining whether the RB is loaded can be obtained (Shi et al., 2020):

$$D_{j\lim} = \frac{e^2 + R_o^{\ 2} - R_i^{\ 2} - 2eR_o\left(\psi_j - \psi_e\right)}{R_o + R_i - e\left(\psi_j - \psi_e\right)} \quad (6)$$

Where ψ_e is the eccentricity angle of the inner ring; When $D_j \geqslant D_{j\lim}$, the jth RB bears the load.

When the RB moves along the raceway, it will contact with the front or rear end of the cage pocket hole, as shown in Fig.1, and the relative displacement and contact force between the RB and the cage can be expressed as (Tu et al., 2021):

$$Q_{cj} = K_c\left(\phi_j - \varphi_c\right)R_m \quad (7)$$

Where K_c is the contact stiffness; φ_c is the curvature of the cage rotation.

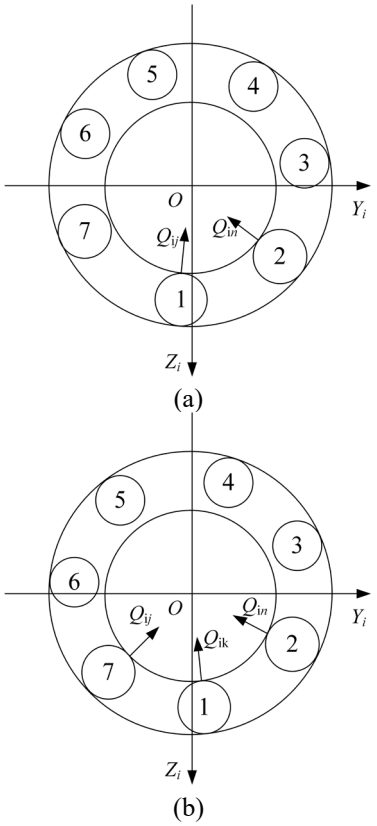

Fig. 3. The situation of different numbers of loaded RBs in the bearing area (a) N=2 (b) N=3

The Traction Force between RB and Raceway under Starved Lubrication

When the required lubricant between the RB and the raceway is not replenished in time, the contact surfaces are in a starved state, as shown in Fig.4. When the RB and raceway are in starved condition, due to the existence of micro-asperity contact friction between the two surfaces, which will affect the force relationship between the two contact surfaces, and need to calculate the oil film thickness and traction force under starved condition. The oil film thickness and traction force under starved condition are calculated as (Wen et al., 2023):

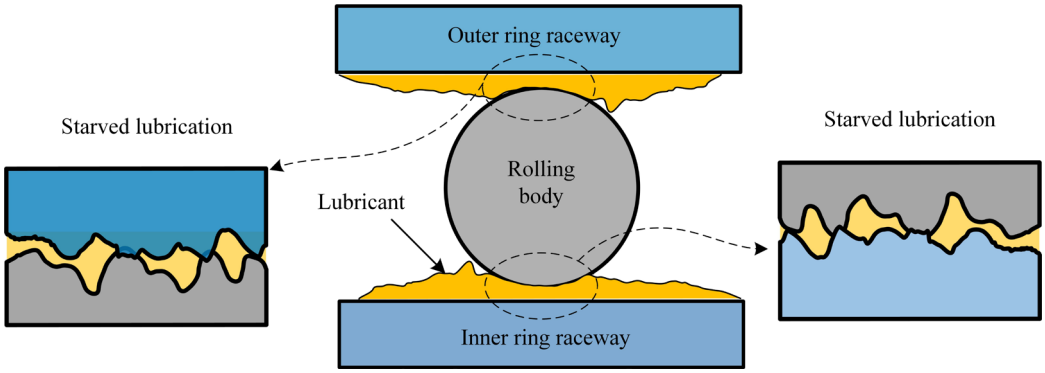

Fig. 4. Schematic of the contact surface between the RB and the raceway.

$$h_c = 3.672R_y W^{-0.045\kappa^{0.18}} U^{0.663\kappa^{0.025}} G^{0.502\kappa^{0.064}} \times\left(1+0.025\overline{\sigma}^{1.248} V^{0.119} W^{-0.133} U^{-0.884} G^{-0.977} \kappa^{0.081}\right) \times\left(1-0.573e^{-0.74\kappa}\right) \quad (8)$$

$$\left(h_c\right)_{\text{starved}} = \left(1-1.561\chi^{0.849}\kappa^{-0.214}\right)\times h_c \quad (9)$$

$$\chi = 1-\frac{\dot{m}_s}{\dot{m}_f} \quad (10)$$

Where h_c is the film thickness in fully EHL; $(h_c)_{\text{starved}}$ is the film thickness in the state of starved lubrication; U, G, W and V is the dimensionless parameter of the system; κ is the ellipticity coefficient; χ denotes the degree of starvation; $\dot{m}_s$ and $\dot{m}_f$ is the lubricant mass flow rate under starved conditions and fully EHL conditions, respectively.

The asperity contact ratio $L_{\text{a-starved}}$ of the micro-convex body between the RB and the raceway is calculated as (Wen et al., 2023):

$$L_{\text{a-starved}} = 10W^{-0.083}U^{0.143}G^{0.314} \times\left[\ln\left(1+\left(1-\chi\right)^{-7.326}\overline{\sigma}^{4.689} V^{0.509} W^{-0.501} U^{-2.9} G^{-2.87}\right)\right] \quad (11)$$

After quantifying the asperity contact ratio, the pressure distribution between the RB-raceway can be further determined:

$$\begin{cases} P_a = P_{\max}\dfrac{L_{\text{a-starved}}}{100} \\ P_h = P_{\max}\left(1-\dfrac{L_{\text{a-starved}}}{100}\right) \end{cases} \quad (12)$$

Where $P_{\max}$ is the maximum contact pressure between the RB and the raceway contact surface; P_a is the contact pressure borne by the micro-asperity body; P_h is the contact pressure borne by the oil film.

Therefore, the traction force between the RB and the raceway can be calculated as (Wen et al., 2023):

$$\tau(x',y') = \min\left[\eta(x',y')\Delta V/\left(h_c\right)_{\text{starved}}, \Lambda\times P_h\right] + f_c P_a \quad (13)$$

$$F_{i/oj} = \iint \tau(x',y')\mathrm{d}x'\mathrm{d}y'$$

where $\tau_{(x',\,y')}$ is the oil film shear stress; $\eta_{(x',\,y')}$ is the lubricant viscosity; ΔV is the sliding velocity between the RB and raceway; Λ is the ultimate shear stress coefficient; and f_c denotes the roughness friction coefficient.

Establishment of Bearing Motion Model

According to Hertz theory and the geometric model of bearing in Fig.1, the motion of the inner ring can be described as:

$$\begin{aligned} W_y - \sum_{N_b}^{i=1}\left(Q_{ij}\cos\phi_j - F_{ij}\sin\phi_j\right) - m_i\frac{\mathrm{d}^2 y}{\mathrm{d}t^2} = c\frac{\mathrm{d}y}{\mathrm{d}t} \\ W_z - \sum_{N_b}^{i=1}\left(Q_{ij}\sin\phi_j + F_{ij}\cos\phi_j\right) - m_i\frac{\mathrm{d}^2 z}{\mathrm{d}t^2} = c\frac{\mathrm{d}z}{\mathrm{d}t} \end{aligned} \quad (14)$$

Where c is damping.

The motion of a RB can be described as:

$$\begin{aligned} F_{ij} - F_{oj} - Q_{cj} - m_r g\cos\psi_j - m_r R_m\frac{\mathrm{d}\omega_{mj}}{\mathrm{d}t} = 0 \\ \left(F_{ij}+F_{oj}\right)R_r - m_r R_m\omega_{mj}^{\ 2}R_r - m_r R_r^{\ 2}\frac{\mathrm{d}\omega_{rj}}{\mathrm{d}t} = 0 \end{aligned} \quad (15)$$

Where ω_{mj} is the circumferential angular velocity of the jth RB:

$$\omega_{mj} = \frac{\mathrm{d}\phi_j}{\mathrm{d}t} \quad (16)$$

The motion of the cage can be described as:

$$R_m\sum_{N_b}^{i=1}Q_{cj} - J_c\frac{\mathrm{d}\omega_c}{\mathrm{d}t} = 0 \quad (17)$$

Where J_c is the moment of inertia of the cage.

NUMERICAL SIMULATION

To study the slipping phenomenon and corresponding dynamic characteristics of rolling bearings under different lubrication states, the established rolling bearing starved lubrication dynamics model is numerically solved. The 6304 deep groove ball bearing is taken as an example for the study, and the parameters of the bearing and the performance parameters of the lubricant are shown in Table 1. The operating temperature is 40 °C, radial load W=100 N, inner ring speed ω_i=4000 r/min.

Table 1. Main parameters of rolling bearing

Parameters	Value
Outer raceway radius R_o(mm)	22.77
Inner raceway radius R_i(mm)	13.24
Bearing pitch circle radius R_m(mm)	18
RB radius R_r(mm)	4.76
Number of RBs N_b	7
Radial clearance ε(mm)	$1\times\mathbf{10^{-3}}$
Raceway surface roughness σ_1(μm)	0.028
Surface roughness of the ball σ_2(μm)	0.042
Material cypress pine ratio v	0.3
Density of lubricant ρ(Kg/m3)	826
Lubricant in viscosity η_0(Pa·s)	0.04
Ultimate shear stress coefficient Λ	0.0434

Assuming that there is a worn RB with the radius of 4.71 mm in the bearing, the above analysis indicates that there may be 2-3 load-bearing RBs in the bearing area. The analysis of sliding effect and force in this paper is based on the worn RB. This study defined the rotational motion of the inner ring, RE, and cage, resulting in a second-order nonlinear ordinary differential equation. Using a fixed time step (Δt=5×$\mathbf{10^{-4}}$) fourth-order Runge-Kutta algorithm to solve differential equation systems

The influence of different starved lubrication degree on the lubrication state of the faulty rolling bearing can be obtained by solving the kinetic model, as shown in Fig.5. From Fig.5, the RB enters the contact zone when the azimuth angle around ϕ_j=300° , and the oil film thickness decreases under the radial load, and it can be clearly observed that the oil film thickness between the RB and the raceway decreases with the increase of the starved lubrication degree.

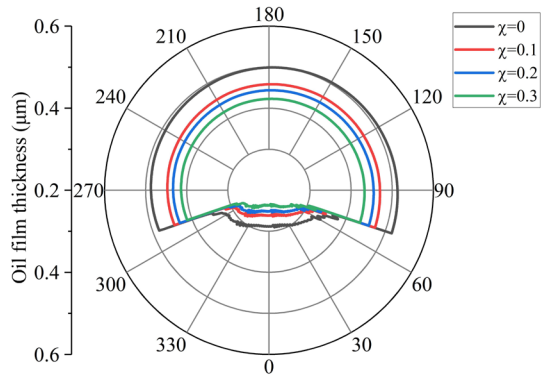

Fig. 5. The influence of starved lubrication on oil film thickness

The rotational velocities of RBs and cages as well as the RB-raceway slip velocities are shown in Fig.6. The increase in the degree of starved lubrication leads to an increase in the friction between the RB-raceway, which drives the RB to rotate around the center of the bearing at an increased rate, i.e., the rotational speed of the RB and cage increases with the increase in the degree of starved lubrication, as shown in Fig.6(a),(b). Fig.6(c) shows the RB-raceway slip velocity, in the contact zone the RB is subjected to radial load, so the slip velocity decreases rapidly. In addition it can be clearly observed that the slip rate decreases rapidly with the increase of the starved degree within one week of RB rotation.

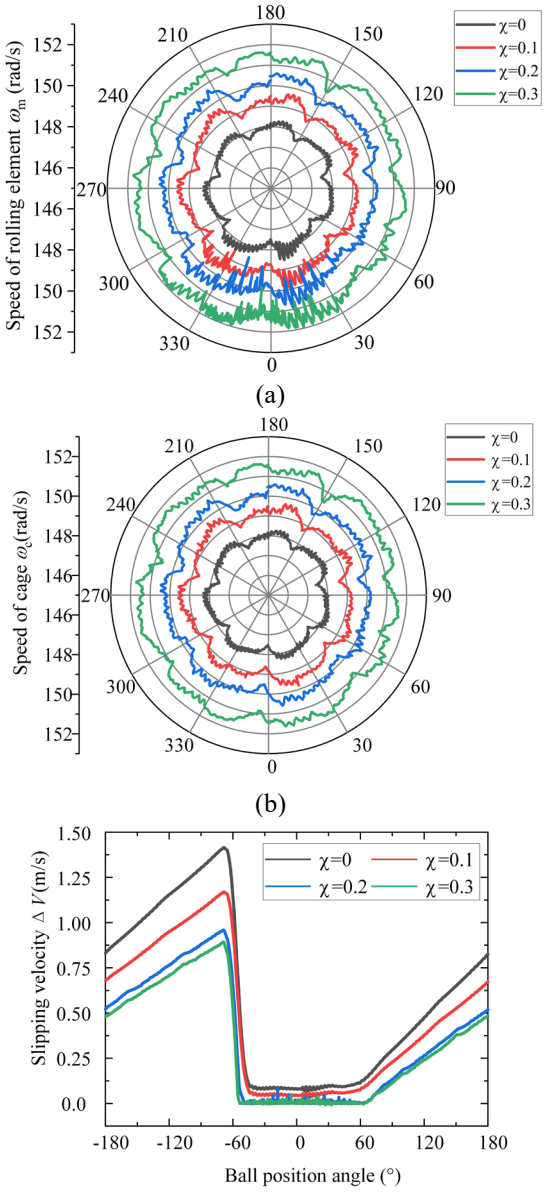

Fig. 6. Influence of starved lubrication on bearing speed (a) revolution speed of RB (b) cage speed (c) sliding speed of RB to raceway

Fig.7(a) shows the contact forces between the RBs and the raceway of the ball bearing without considering the wear of the RBs. The contact forces of each RB in the non load zone are zero, and the contact forces of each RB in the load zone are almost equal. The appropriate value range of the degree of

starved lubrication χ in the starved lubrication theory of point contact bearings is 0 to 0.3. Fig.7(b) - (d) show the variation of contact force between each RB and raceway at different χ values of 0.1, 0.2, and 0.3. Due to the wear and tear of ball 3, there is a diameter difference compared to other balls, and it experiences less contact force than the other balls. The contact force on adjacent balls 2 and 4 increases compared to when the wear of RBs is not considered, which reflects the uneven bearing load effect caused by the wear of RBs. As χ increases, the thickness of the oil film inside the bearing decreases, and the contact stiffness increases, resulting in an overall upward trend of contact forces on each RBs (Wang et al, 2022).

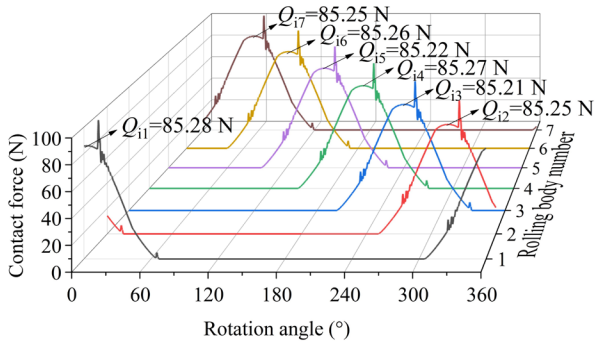

(a)

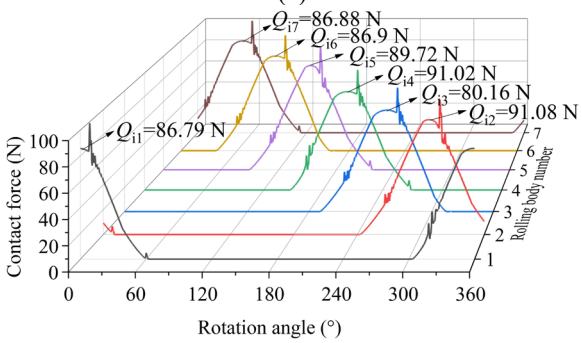

(b)

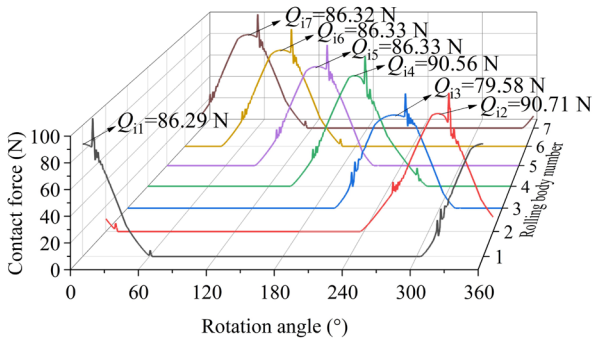

(c)

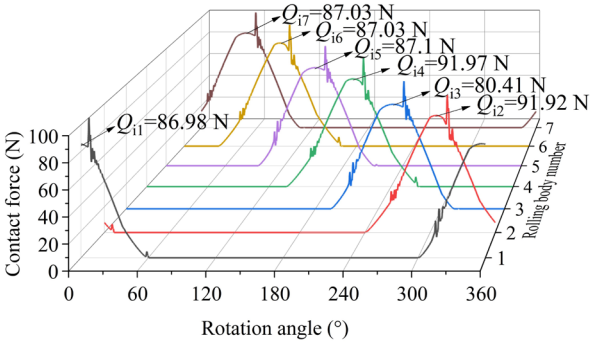

(d)

Fig. 7. Contact force between RB and raceway under different degrees of starved lubrication (a) χ=0 (b) χ=0.1 (c) χ=0.2 (d) χ=0.3

Eq. (18) provides the calculation method for the friction torque between the RB and the raceway. Fig.8 shows the variation of friction torque for different degrees of starved lubrication. The curves A, B, C, and D represent the depleted oil conditions at χ=0, 0.1, 0.2, and 0.3, respectively. After the wear of the RBs, as the degree of starved lubrication increases, the friction torque increases. In addition, changes in friction torque can affect the degree of bearing sliding. According to Tu (Tu et al., 2019), the more sufficient the friction between the RB and the raceway, the greater the driving force provided for the RB and the cage, thereby suppressing bearing sliding. With the increase of χ, that is, the increase of friction torque reduces the slip effect, verifying the decrease in slip velocity, which is consistent with Tu's research results. Meanwhile, this also confirms the conclusion in Fig.6 that the sliding effect is suppressed as the degree of starved lubrication increases after the wear of the RB.

$$M_{\mathrm{f,average}} = \mathrm{AVERAGE}\left[\sum_{j=1}^{N_b}\left(F_{ij}R_i + F_{oj}R_o\right)\right] \tag{18}$$

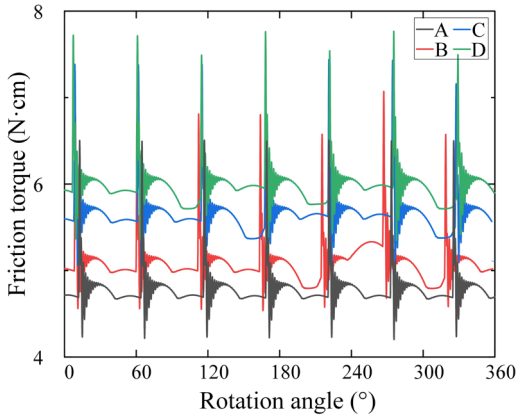

Fig. 8. Friction torque between RB and raceways under different degrees of starved lubrication

The spectrum of Fig.9 was obtained by solving the differential equation. Nf_r is the rotational frequency, where $nf_{cA,B,C,D}$ correspond to the rotational frequency and doubling frequency of the cage under four lubrication states, while $f_{bwA,B,C,D}$ correspond to the characteristic frequencies of RB wear faults. According to Shi's research (Shi et al., 2020), when uneven load bearing effects occur inside the bearing, a fractional multiple of the cage frequency f_c, f_{cw}=3f_c/N, appears on the spectrum. And when there is 1,2... N/3 loaded RB in the bearing area, the corresponding characteristic frequencies are f_{cw}, 2f_{cw},... Nf_{cw}/3. For the bearings selected in this paper, there are 7 RBs, and there may be 3 loaded RBs simultaneously in the bearing area. When the worn RBs enter the bearing area, there are 2 loaded RBs in the bearing area, and the corresponding characteristic frequency on the spectrum is 2f_{cw}; After the worn RB leaves the bearing area, there are three loaded RBs in the bearing area. At this time, 3f_{cw}>f_c, and the load-bearing characteristics of bearings after RB wear will appear as f_c and its harmonic components. Therefore, the characteristic frequency of 2f_{cw} can be sufficient to determine whether the rolling body wear fault occurs, and it is expressed in the spectrum by f_{bw}.

As the degree of starved lubrication, the friction torque between the RB and the raceway increases, and the sliding effect is suppressed. This is manifested by an increase in the rotational frequency f_c and its harmonic component nf_c of the cage, but still lower than the theoretical value of ideal conditions. The spectrum shows an increase in f_{cA}, f_{cB}, f_{cC}, and f_{cD}, corresponding to an increase in the RB wear frequency f_{bwA}, f_{bwB}, f_{bwC}, and f_{bwD}, as shown in Fig.9.

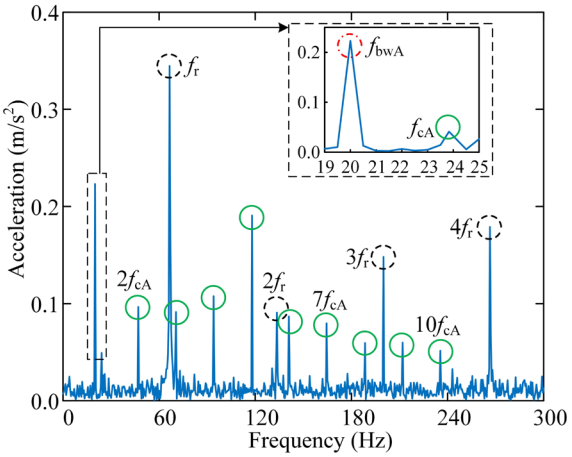

(a)

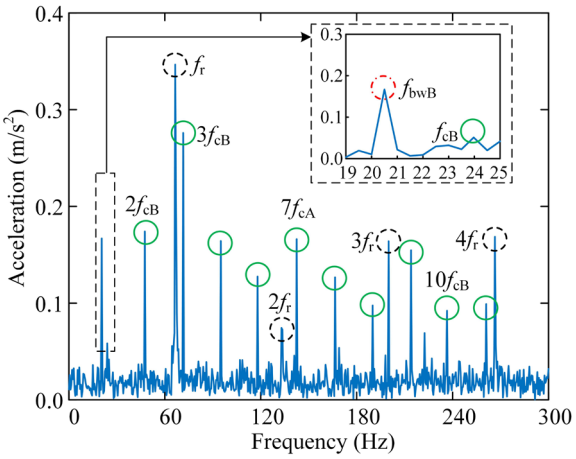

(b)

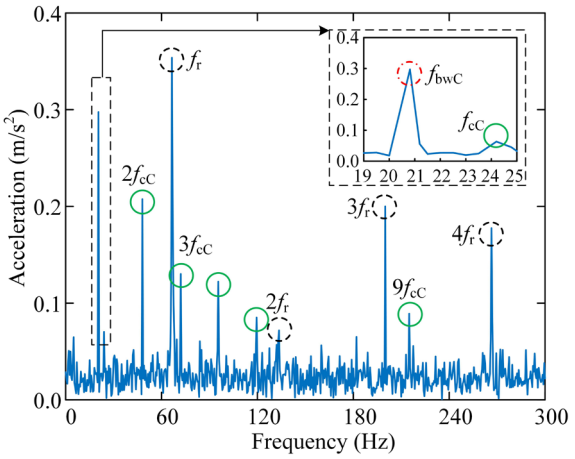

(c)

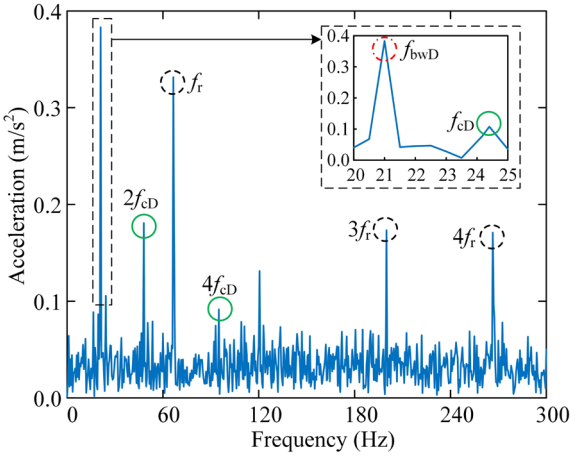

(d)

Fig. 9. Vibration spectrum of bearing dynamics model simulation (a) oil conditions of A (b) oil conditions of B (c) oil conditions of C (d) oil conditions of D

Table 2 shows the frequency values of the cage rotation frequency and RB wear characteristic frequency in Fig.9, and significant frequency changes

can be observed. This indicates that when monitoring the wear of RBs, it is necessary to consider the actual state of starved lubrication, in order to achieve more accurate monitoring of the wear status of RBs.

Table 2 Characteristic frequencies at different degrees of starved lubrication

Item	χ=0	χ=0.1	χ=0.2	χ=0.3	Change rate
f_c (Hz)	23.85	23.96	24.18	24.3	1.9 %
f_{bw} (Hz)	20.2	20.37	20.78	20.91	3.5 %

EXPREIMENTAL STUDY

For verifying the correctness of the model proposed in this paper and detect the bearing vibration characteristics of RB wear fault under starved lubrication, an experimental setup as shown in Fig.10 was established in this section. In Fig.10, the speed was controlled by a speed controller, and the motor output speed was from 0 to 5000 r/min. The vibration signal was obtained by a contact type acceleration sensor arranged on the bearing seat and further processed by a data collector, with a sampling frequency of 5000 Hz. The selected bearing were consistent with those in the simulation in the previous section. Through special customization and procurement, a RB had a radius of 4.71 mm, while the other RBs had a radius of 4.76 mm. This paper designed three sets of experiments P, Q, and R. By manually adding or removing lubricants, the lubricants in the bearing cavity during the three sets of experiments were 0 %, 33 %, and 75 % of the cavity volume, respectively, to simulate changes in the degrees of starved lubrication.

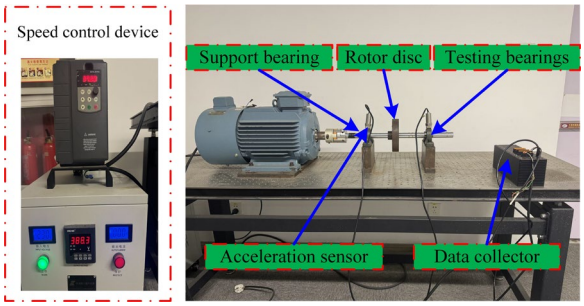

Fig. 10. Experimental testing system

Set the motor output speed to 4000 r/min, collect vibration data after the speed stabilizes, and perform Fourier transform on the vibration signal to obtain the spectrum of the right bearing as shown in Fig.11. On the spectrum, it is clear to see the changes in the characteristic frequencies $f_{cwP,Q,R}$ of RB wear caused by changes in lubricant supply, while the frequency values of the rotational frequency f_r and its harmonic components related to input speed remain unchanged. In the P, Q, and R tests, the corresonding RB wear characteristic frequencies were 19.47 Hz, 20.05 Hz, and 21.51 Hz, respectively. The corresponding cage rotation frequency and its harmonic components were also excited. However, due to frequency modulation and mutual influence, the amplitude of the first harmonic frequency $f_{cP,Q,R}$ of the cage rotation was relatively low, which may be submerged in background noise in practice. However, the RB wear characteristic frequencies still vary significantly.

Compared with simulation, it is difficult to accurately simulate the increase and decrease of lubricants. However, this experiment still verified the hypothesis that the characteristic frequency changed with the degrees of starved lubrication, and quantified the characteristics of RB wear fault under different degrees of starved lubrication, proving the correctness of the theoretical model and calculation.

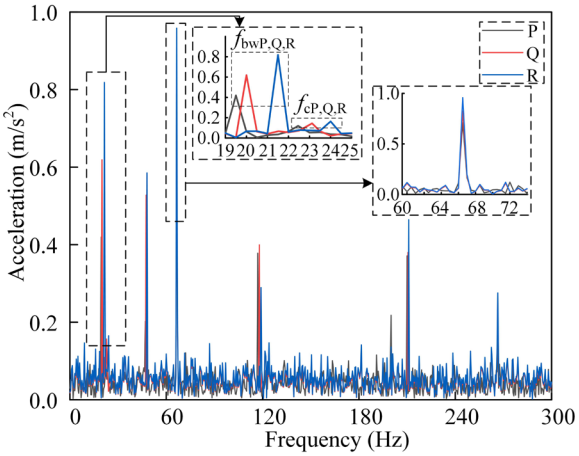

Fig. 11. Frequency curve of experimental data

CONCLUSIONS

This paper considered the wear failure of bearing RBs caused by bearing starved lubrication, and quantified the degree of RB wear through diameter tolerance. By adjusting the oil supply, the frequency characteristics of RB wear failure under different lubrication degrees were achieved. The main conclusions are as follows:

(1) When the wear of RB occurs, the bearing exhibited a significant uneven load bearing effect, manifested as a small contact force acting on the worn RB and a large contact force acting on adjacent RBs;

(2) An increase in the degree of starved lubrication would cause a decrease in the thickness of the oil film, an increase in contact stiffness, and thus an increase in contact force;

(3) As the lubrication degrees of the starved lubrication increased, the friction between the RB and the raceway increased, and the larger friction torque would become the driving force to promote the rotation of the cage and RB, thereby suppressing the sliding effect of the bearing;

(4) After the occurrence of a RB wear fault, the frequency component related to the fractional frequency of the cage would appear on the spectrum, and the specific frequency value was related to the total number of RBs. This characteristic frequency changed significantly with the degrees of starved lubrication, and should be fully considered during fault monitoring. The research results provide rich theoretical basis for the precise monitoring and diagnosis of rolling bearings in practice.

ACKNOWLEDGMENT

Financial support for this work was provided by the the Science and Technology Research Project of Hebei Provincial Department of Education (Grant No. QN2022185).

REFERENCES

Bai, X. T., Wu, Y. H., Rosca, I. C., Zhang, K., and Shi, H. T., "Investigation on the effects of the ball diameter difference in the sound radiation of full ceramic bearings," Journal of Sound and Vibration, Vol. 450, pp. 231-250(2019). DOI: 10.1016/j.jsv.2019.02.015.

Bian, Z., Song, C., Meng, L. H., and Zhou, Q. H., "Response of the interface between the ball and the raceway of rolling bearing under starved lubrication," IOP Conference Series: Materials Science and Engineering, Vol. 1043, No. 5, pp. 052005(2021). DOI: 10.1088/1757-899X/1043/5/052005.

Cao, H., Shi, F., Li, Y., Li, B., and Chen, X., "Vibration and stability analysis of rotor-bearing-pedestal system due to clearance fit," Mechanical Systems and Signal Processing, Vol. 133, pp. 106275(2019). DOI: 10.1016/j.ymssp.2019.106275.

Jiang, Y., Huang, W., Luo, J., and Wang, W., "An improved dynamic model of defective bearings considering the three-dimensional geometric relationship between the rolling element and defect area," Mechanical Systems and Signal Processing, Vol. 129, pp. 694-716(2019). DOI: 10.1016/j.ymssp.2019.04.056.

Liu, Y., Wang, W., Qing, T., Zhang, Y., Liang, H., and Zhang, S., "The effect of lubricant temperature on dynamic behavior in angular contact ball bearings," Mechanism and Machine Theory, Vol. 149(2020). DOI: 10.1016/j.mechmachtheory.2020.103832.

Liu, Y., Chen, Z., Li, Y., Zhai Wanming %+ State Key Laboratory of Traction Power, S. J. U. C. P. s. R. o. C., and School of Mechanical Engineering, S. J. U. C. P. s. R. o. C., "Dynamic investigation and alleviative measures for the skidding phenomenon of lubricated rolling bearing under light load," Mechanical Systems and Signal Processing, Vol. 184(2023).

Maruyama, T., and Saitoh, T., "Relationship between Supplied Oil Flow Rates and Oil Film Thicknesses under Starved Elastohydrodynamic Lubrication," Lubricants, Vol. 3, No. 2, pp. 365-380(2015). DOI: 10.3390/lubricants3020365.

Qin, Y., Cao, F., Wang, Y., Chen, W., and Chen, H., "Dynamics modelling for deep groove ball bearings with local faults based on coupled and segmented displacement excitation," Journal of Sound and Vibration, Vol. 447, pp. 1-19(2019). DOI: 10.1016/j.jsv.2019.01.048.

Shi, H. T., and Bai, X. T., "Model-based uneven loading condition monitoring of full ceramic ball bearings in starved lubrication," Mechanical Systems and Signal Processing, Vol. 139(2020). DOI: 10.1016/j.ymssp.2019.106583.

Shi, X., Lu, X., Feng, Y., and Qiu, Z., "Tribo-dynamic analysis for aero ball bearing with 3D measured surface roughness," Engineering Failure Analysis, Vol. 131, pp. 105848(2022). DOI: 10.1016/j.engfailanal.2021.105848.

Tu, W., Luo, Y., Yu, W., and Yu, Y., "Investigation of the dynamic local skidding behaviour of rollers in cylindrical roller bearings," Proceedings of the Institution of Mechanical Engineers, Part K: Journal of Multi-body Dynamics, Vol. 233, No. 4, pp. 899-909(2019). DOI: 10.1177/1464419319861616.

Tu, W., Yu, W., Shao, Y., and Yu, Y., "A nonlinear dynamic vibration model of cylindrical roller bearing considering skidding," Nonlinear Dynamics, Vol. 103, No. 3, pp. 2299-2313(2021). DOI: 10.1007/s11071-021-06238-0.

Visnadi, L. B., and De Castro, H. F., "Influence of bearing clearance and oil temperature uncertainties on the stability threshold of cylindrical journal bearings," Mechanism and Machine Theory, Vol. 134, pp. 57-73(2019). DOI: 10.1016/j.mechmachtheory.2018.12.022.

Wang, Y., Yan, C., Lu, Z., Liu, Y., and Wu, L., "Effect of thermal elastohydrodynamic lubrication on vibration characteristics of ball bearing with local defect," Proceedings of the Institution of Mechanical Engineers, Part K: Journal of Multi-body Dynamics, Vol. 236, No. 3, pp. 488-500(2022). DOI: 10.1177/14644193221095438.

Wang, Z., Yu, Q., Shen, X., and Chen, X., "A Simple Model for Scuffing Risk Evaluation of Point Contact Under Mixed Lubrication," Journal of Tribology, Vol. 140, No. 3(2018). DOI: 10.1115/1.4038410.

Wen, C., Meng, X., Gu, J., Xiao, L., Jiang, S., and Bi, H., "Starved lubrication analysis of angular contact ball bearing based on a multi-degree-of-freedom tribo-dynamic model," Friction, Vol. 11, No. 8, pp. 1395-1418(2023). DOI: 10.1007/s40544-022-0661-2.

APPENDIX

I. Theoretical rotational speed ω_{ct} of the cage revolution.

$$\omega_{ct} = \frac{\omega_i d_i + \omega_o d_o}{2 d_m}$$

II. Cage moment of inertia J_c.

$$J_c = \frac{m_c R_m^{\ 2}}{2}$$

NOMENCLATURE

m_c Cage mass

m_r Mass of the rolling body

W_y Radial loads along the *Y*-axis

W_z Radial loads along the *Z*-axis,

θ_j The initial position angle of the *j*th rolling body

球轴承滚动体在乏油润滑下的滑动磨损特征研究

霍忠堂　陳建奇　郝玲娟　高建松
邯鄲學院機電學院

摘 要

球軸承長期運轉導致潤滑條件惡化形成的乏油潤滑狀態，加劇滾動躰的磨損，準確識別該故障對軸承狀態監測影響重大。本文以直逕差量化滾動躰的磨損，考慮了部件間的摩擦，建立了乏油條件下滾動躰磨損的故障動力學模型，探索了滾動躰磨損的機理，獲取了滾動躰磨損後的頻率特征。模擬和實驗結果表明，乏油程度增大，雖然可以抑制滑動傚應，但增大的摩擦將加劇滾動躰的磨損；頻域中保持架鏇轉頻率的分數倍頻可以作爲監測滾動躰磨損程度與個數的依據，此外，乏油程度的改變將直接影響保持架鏇轉頻率，但仍可用架鏇轉頻率的分數倍頻來對滾動躰磨損故障進行識別。模型的提出與驗證，為實現實際工況中軸承的精準監測與定性診斷提供了有價值的參考。